JGR Oceans

RESEARCH ARTICLE
10.1029/2019JC015761

Key Points:
- A numerical model reproduces key elements of the South-East Madagascar Bloom
- Importance of horizontal advection of fresher nutrient-rich waters from Madagascan coast is shown
- Atmospherically triggered phytoplankton bloom is evident in both the model and observations

Correspondence to:
A. F. Dilmahamod,
fehmi.dilmahamod@gmail.com

Citation:
Dilmahamod, A. F., Penven, P., Aguiar-González, B., Reason, C. J. C., & Hermes, J. C. (2020). A model investigation of the influences of the South-East Madagascar current on the South-East Madagascar bloom. *Journal of Geophysical Research: Oceans*, *125*, e2019JC015761. https://doi.org/10.1029/2019JC015761

Received 11 OCT 2019
Accepted 4 MAY 2020
Accepted article online 7 MAY 2020

A Model Investigation of the Influences of the South-East Madagascar Current on the South-East Madagascar Bloom

A. F. Dilmahamod[1,2,3,4,5], P. Penven[2], B. Aguiar-González[3,6], C. J. C. Reason[1], and J. C. Hermes[1,3,7]

[1]Department of Oceanography, University of Cape Town, Cape Town, South Africa, [2]Université de Bretagne Occidentale, CNRS, IRD,Ifremer, Laboratoire d'Océanographie Physique et Spatiale (LOPS), IUEM, Brest, France, [3]Egagasini Node, South African Environmental Observation Network, Cape Town, South Africa, [4]Now at GEOMAR Helmholtz Centre for Ocean Research Kiel, Kiel, Germany, [5]Now at Department of Oceanography, Dalhousie University, Halifax, Nova Scotia, Canada, [6]Departamento de Fisica, Facultad de Ciencias del Mar, Universidad de Las Palmas de Gran Canaria, Las Palmas, Spain, [7]Ocean Sciences Department, Nelson Mandela University (NMU), Port Elizabeth, South Africa

Abstract The South-East Madagascar Bloom, one of the most compelling biogeochemical features of the Indian Ocean, occurs sporadically during austral summer in the oligotrophic waters south-east of Madagascar, where it can cover up to 1% of the global ocean surface area. Its spatial extension and its timing are highly variable. A high-resolution biophysical model is used to investigate a previous hypothesis that the onset of a particular circulation of the South-East Madagascar Current advects fresher and nutrient-rich waters eastward, feeding the bloom. The model is able to reproduce an intermittent phytoplankton bloom with large spatial variability but in the subsurface layers, as well as the presence of an irregular retroflection of the South-East Madagascar Current. The simulated bloom occurs within a shallow stratified mixed layer, with fresher waters at the surface, parallel to the water mass in an observed bloom. The model results suggest, from a nutrient flux analysis, that horizontal advection of low-salinity nutrient-rich Madagascan coastal waters can indeed trigger a phytoplankton bloom. The coupled model is also able to resolve a bloom that is atmospherically forced by cyclonic activity.

1. Introduction

A unique and intriguing aspect of the biologically oligotrophic South-West Indian Ocean is the occurrence of a sporadic enhancement of chlorophyll-a (Chl-a) concentration, namely, the South-East Madagascar Bloom (Longhurst, 2001). Prevailing in austral summer, this dendritic feature varies remarkably in terms of its initiation and termination month, as well as its spatial extent (Dilmahamod et al., 2019; Wilson & Qiu, 2008). With respect to ocean biology, it has been referred to as one of the most compelling features of interannual variability, after El Niño Southern Oscillation (ENSO) (Uz, 2007). A fully developed South-East Madagascar Bloom exhibits Chl-a surface concentration of 1 mg/m^3, with some patches reaching 2–3 mg/m^3 (Longhurst, 2001). It can extend from the Madagascan coast up to 70°E, covering ~1% of the world's ocean surface area (Srokosz & Quartly, 2013). This ecological hotspot occurs in the exclusive economic zone (EEZ) of the surrounding islands and hence can potentially be of particular importance to their marine resources. Additionally, it can be influential for biogeochemical cycling of elements (Naik et al., 2015) and the uptake of atmospheric carbon dioxide (CO_2) (Lévy et al., 2012; Sapiano et al., 2012). Nonetheless, a paucity of continuous *in situ* data has hindered any plausible explanations for the formation mechanisms of this bloom.

Previous studies, with different outcomes, have addressed the physical mechanisms responsible for the onset and distribution of the bloom (Dilmahamod et al., 2019; Huhn et al., 2012; Lévy et al., 2007; Longhurst, 2001; Raj et al., 2010; Srokosz et al., 2004, 2015; Srokosz & Quartly, 2013; Uz, 2007), but none have been as yet clearly substantiated. A review of what is currently known was first proposed by Srokosz and Quartly (2013) and was extended and expanded by Dilmahamod et al. (2019). This exhaustive analysis was made possible through a 19-year data set of ocean color and other prolonged observational data sets. Dilmahamod et al. (2019) proposed a novel bloom index that provides an improved insight on the timing and intensity of the bloom. The index is based on the Chl-a difference between the bloom box (24–30°S; 48–66°E, Uz, 2007) and a similarly-sized box further offshore. Eleven bloom years (1999, 2000, 2002, 2004, 2006, 2008,

2009, 2011, 2012, 2013, and 2014) were identified, from which three were described as major bloom years (1999, 2006, and 2008). The bloom was found to prevail within a low-salinity, shallow stratified mixed layer, consistent with Uz (2007) and Srokosz and Quartly (2013), with temperatures exceeding 24.8°C and excess light availability (Raj et al., 2010). These are the ideal conditions for nitrogen-fixing cyanobacteria, namely, *Trichodesmium*, to thrive (Capone et al., 1997; Hood et al., 2001, 2004; Wilson & Qiu, 2008). Several studies have argued the predominance of nitrogen-fixing cyanobacteria in the South-East Madagascar Bloom (Poulton et al., 2009; Srokosz & Quartly, 2013; Uz, 2007). The biogeography and activity of *Trichodesmium* is, however, often constrained by iron availability (Berman-Frank et al., 2001; Hood et al., 2000), and since the concerned region is an area of minimum dust deposition (Wilson & Qiu, 2008), the possibility of the South-East Madagascar Bloom consisting of organisms other than nitrogen fixers should not be excluded.

The current-induced coastal upwelling south-east of Madagascar (Lutjeharms & Machu, 2000; Machu et al., 2002; Ramanantsoa et al., 2018) was presented as the main mechanism triggering and controlling the interannual variability of the bloom (Lévy et al., 2007; Raj et al., 2010; Srokosz & Quartly, 2013). Hence, it is expected that the bloom would be associated with an enhanced upwelling intensity, bringing more nutrients (Lévy et al., 2007; Raj et al., 2010) or dissolved iron (Srokosz & Quartly, 2013) into the surface layers. However, the quantitative assessment performed by Dilmahamod et al. (2019) presented a clear contradiction to this theory, showing that the bloom coincided with a dampening of the upwelling intensity. The same analysis revealed co-occurrences of bloom events with the mature phase of La Niña, 91% of the time (10 out of 11 events). A connection between La Niña, reduced upwelling south-east of Madagascar, and the South-East Madagascar Bloom was proposed, stating that an increased South Equatorial Current (SEC) during La Niña (Palastanga et al., 2007; Yamagami & Tozuka, 2015) will result in a stronger South-East Madagascar Current (SEMC), hence favoring a detachment of the current from the coast, following Ou and de Ruijter (1986). These two SEMC pathways, towards the Agulhas Current and alternatively feeding into the South Indian Ocean Countercurrent (SICC), are in agreement with Siedler et al. (2009). This detachment creates a pathway for low-salinity, nutrient-rich coastal waters towards the bloom region. Consequently, the current driving the coastal upwelling south-east of Madagascar is weakened, reducing the upwelling intensity during bloom phenomena (Dilmahamod et al., 2019).

This study aims to model, for the first time, the South-East Madagascar Bloom using a 21-year (1993–2013) high-resolution coupled biophysical model. In line with the hypothesis put forward by Dilmahamod et al. (2019), the possible influences of the local perturbations of the SEMC on the bloom are explored. A sporadic enhancement of simulated Chl-a concentration is observed during austral summer, within the subsurface layers, in the bloom region. This subsurface bloom displays quite similar characteristics as the observed bloom. This paper proceeds as follows: the observational data and model configuration, as well as the ability of the model to resolve the physical/biogeochemical processes, are described in section 2; the temporal, spatial, and vertical characterization of the simulated bloom are reported in section 3; section 4 provides an analysis of the possible intrusion of SEMC waters into the Madagascar Basin; and sections 5 and 6 discuss and conclude the study.

2. Data and Methods

2.1. Satellite Data

Remotely-sensed surface Chl-a concentration used in this study is provided by the Ocean Color Climate Change Initiative (OC-CCI) (Lavender et al., 2015; Satyendranath et al., 2016) project from the European Space Agency (ESA). It uses band-shifting and bias-corrected techniques to merge data from three ocean-color satellite platforms, namely, MERIS, MODIS, and SeaWiFS, hence providing a continual Chl-a time series from September 1997 to May 2018. The 8-day composites of Level-3 data, at a spatial resolution of ~4.5 km ($\frac{1}{24}°$), were acquired freely on the project website (www.esa-oceancolour.cci.org).

Sea level anomalies (SLAs) and geostrophic current data sets are produced by Copernicus Marine and Environment Monitoring Service (CMEMS; http://marine.copernicus.eu). These are merged products from multiple altimeters (Ducet et al., 2000) and are available as daily output from 1993 until the present, on a 0.25° horizontal grid resolution.

2.2. *In-Situ* Data

The CSIRO Atlas of Regional Seas 2009 (CARS09) provides a comprehensive set of quality-controlled vertical profiles of *in-situ* temperature, practical salinity, nitrate, oxygen, silicate, and phosphate (Ridgway et al., 2002). These are constructed from raw profiles belonging to different databases, including the (i) World Ocean Circulation Experiment (WOCE) Global Hydrographic Program, (ii) World Ocean Database 2005, (iii) Argo global archives up to May 2009, and so on. CARS09 is mapped onto a 0.5° horizontal grid resolution, with 79 standard depths from the sea surface to 5,500 m.

The international Argo Program (Argo, 2000) consists of ~4,000 autonomous Lagrangian profiling floats, which provide freely available temperature and salinity data from the surface down to 2,000 m, every 10 days (Coriolis Project: http://coriolis.eu.org). The Argo Data Centre (Böhme & Send, 2005; Owens & Wong, 2009; Wong et al., 2003) applies an automatic pre-processing and quality control measures, from which two additional criteria based on the quality control flags and sampling characteristics are implemented: (1) only temperature, salinity, and pressure data flagged 1 (good) and 2 (potentially good) were considered and (2) only profiles with at least four data points in the first 50 m, with the shallowest data point being between the surface and 20 m, are examined.

2.3. The SWIO Model Configuration

The oceanic simulation was performed with the Coastal and Regional Ocean Community Model (CROCO; Debreu et al., 2012), which was developed around the Regional Oceanic Modeling System (ROMS; Shchepetkin & McWilliams, 2005). It is a free-surface, terrain-following σ-coordinate model with a split-explicit time-stepping, following the Boussinesq and hydrostatic approximations, and has been designed to realistically resolve basin-scale, regional, and coastal ocean processes at high-resolution (Shchepetkin & McWilliams, 2005). The physical component was coupled with the Pelagic Interaction Scheme for Carbon and Ecosystem Studies version 1 (PISCES-v1) biogeochemical model (Aumont & Bopp, 2006). PISCES can simulate the marine biological productivity and the cycles of carbon as well as the main nutrients (nitrogen, phosphorous, silicate, and iron). It comprises 24 components which include four living components represented by two phytoplankton size classes (nanophytoplankton and diatoms) and two zooplankton size classes (microzooplankton and mesozooplankton). The growth of phytoplankton is limited by five nutrients, namely, nitrate (NO_3), ammonium (NH_4), phosphate (PO_4), silicate (SiO_4), and iron (Fe). Chlorophyll concentration was obtained through the sum of chlorophyll content from nanophytoplankton and diatom (two phytoplankton size classes). The parameters within PISCES-v1 were set to default, as in Aumont and Bopp (2006).

A South-West Indian Ocean (SWIO) configuration was built using the CROCOTOOLS package (Penven et al., 2008), with a parent domain of 0.25° grid, from 0°E to 100.25°E and 5.5°S to 47°S. Within this domain, a 1/12° resolution sub-domain was implemented over the South-East Madagascar Bloom region, extending from 37°E to 80°E and from 18°S to 32°S (red box in Figure 1a). The 45 vertical levels were parameterized for an increased resolution and representation of the upper layer processes, with a minimum vertical discretization of 0.2 m at the surface. The bathymetry was derived from Global Earth Bathymetric Chart of the Oceans (GEBCO1) data. The surface layers of the model were forced using an online interpolation of 0.75° daily ECMWF Re-Analysis data (ERA-Interim; Dee et al. (2011)), from which the variables were used to force a bulk formula representation of surface heat and freshwater fluxes (Fairall et al., 1996). The lateral oceanic forcings were sourced from a non-assimilated Global Ocean Reanalysis (GLORYS) model, known as GLORYS2V3, which has consistent physical and biogeochemical properties. It is based on the ORCA025 (code version: NEMO3.1), with monthly outputs at 0.25° horizontal resolution and 75 vertical z coordinate levels. The physical and biogeochemical components of this configuration, namely, GLORYS2V3-FREE and BIOMER-GLORYS2V3, were available on an overlapping time frame of 21 years (January 1993 to December 2013). A two-way nesting approach was applied, with the larger domain feeding the subdomain and subsequent feedback from the subdomain to the larger one (Debreu et al., 2012). Henceforth, we will refer to the simulation as "SWIO".

The first 3 years (1993–1995) of the boundary forcings data set were replicated on a 1990–1992 time-frame, from which SWIO is initialized as from January 1990. The model is spun up for 3 years until it reaches a quasi-equilibrium state in the upper ocean and is then run for an additional 21 years (1993–2013) with an output delivery frequency of 5 days. The subgrid-scale vertical mixing is set by a non-local K-profile parameterization (Large et al., 1994), with the diffusive part of the lateral advection scheme for tracers rotated along

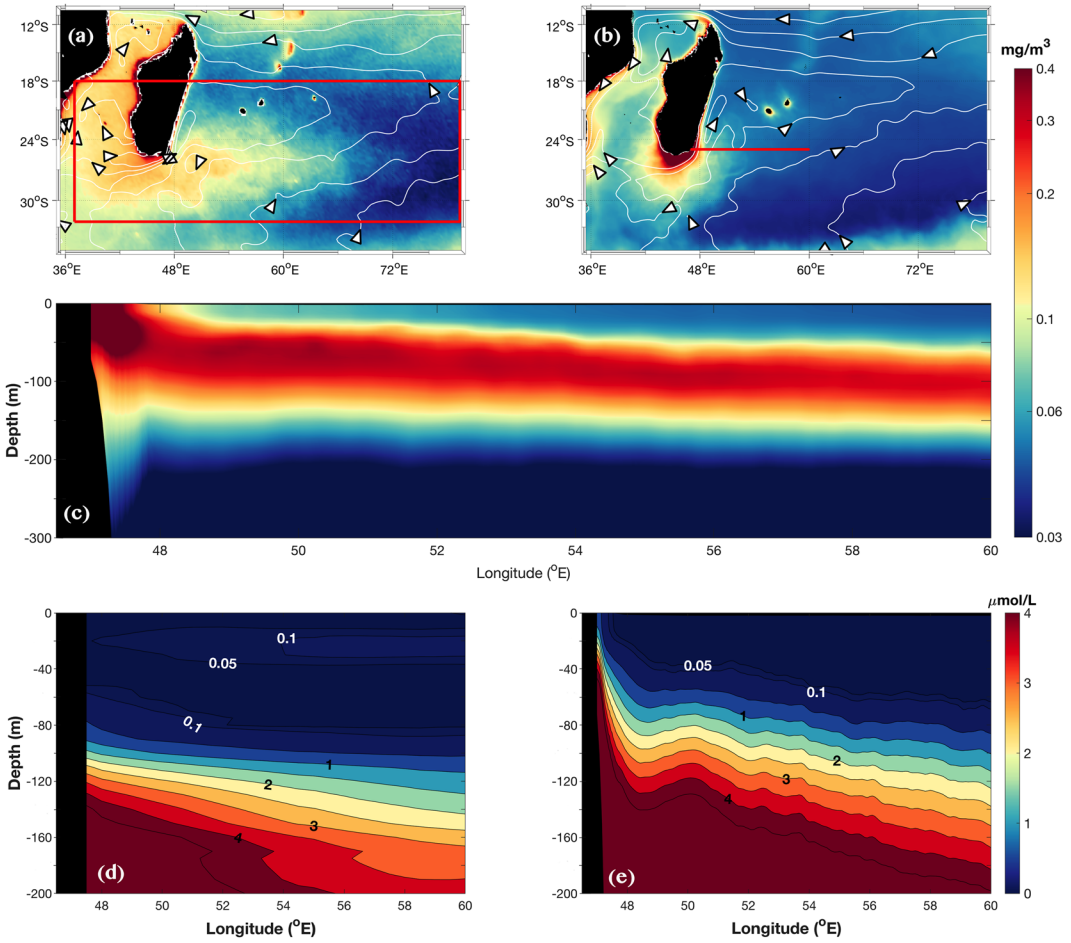

Figure 1. Surface Chl-a concentration (mg/m^3; log scale) from (a) satellite and (b) model data (first 20 m), overlaid with streamlines of sea surface height (SSH) as white lines, plotted every 0.1 m. (c) Vertical structure of modeled Chl-a concentration along a zonal transect at 25°S from 47°E to 60°E. Mean nitrate concentration (μmol/L) from (d) CARS09 climatology and (e) SWIO. Note that (a), (b), (c), and (e) are averaged over January–April from 1998 to 2013, whereas (d) is a mean over January–April CARS09 climatology. The red box in (a) displays the extension of the high-resolution (1/12°) domain, and the red zonal line in (b) shows the zonal section plotted in (c)–(e).

isopycnal surfaces, to prevent spurious diapycnal mixing (Lemarié et al., 2012; Marchesiello et al., 2009). It should be noted that river discharges are not represented in this configuration.

2.4. Model Behavior

The ability of SWIO to adequately resolve the processes in the region needs to be assessed. Simulated Chl-a concentration is averaged over the first 20 m, also known as the "optical depth" or "penetration depth" of satellite sensors (Gordon & McCluney, 1975), and compared with satellite-derived surface Chl-a (Figure 1a). Comparisons were performed over a mean January to April period (1998–2013), with the bloom generally starting in January, peaking in February, and diffusing by March/April (Dilmahamod et al., 2019). An overestimation of coastal Chl-a is observed, confined around the southern Madagascan coast (Figure 1b). The South-East Madagascar Bloom in satellite data is manifested by the mean zonal structure within the 22°–32°S, 50°–70°E region (Figure 1a). A minor zonal extension of simulated Chl-a, up to 55°E, is observed in SWIO although it remains under-estimated compared with satellite ocean color. Reduced simulated surface Chl-a concentration is also observed in the Mozambique Channel, possibly due to a shallower austral summer mixed layer depth in SWIO, in comparison with observations (not shown here). The concentration of phytoplankton cells is over-estimated in austral winter (not shown here), but this period is not considered owing to the bloom being phase-locked to austral summer.

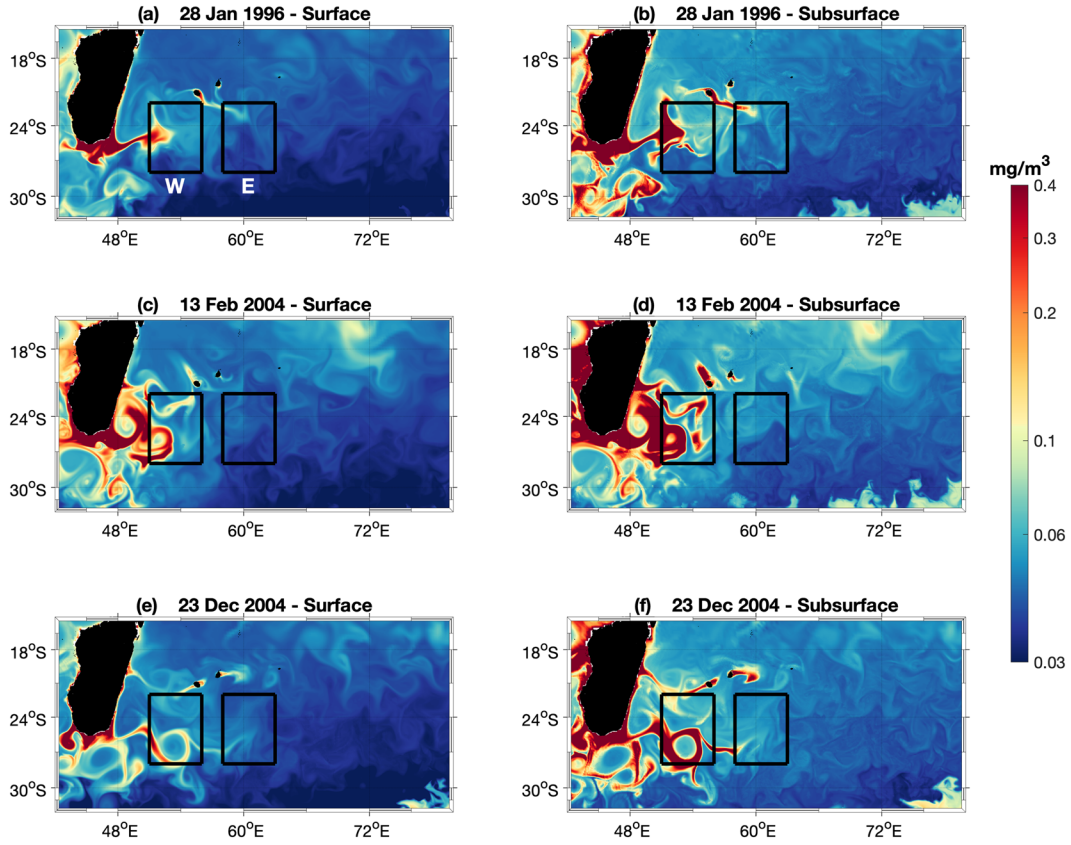

Figure 2. Snapshots of simulated Chl-a concentration (mg/m^3; log scale) in the surface (left panels) and subsurface (right panels) layers for 28th January 1996 (a and b), 13th February 2004 (c and d), and 23rd December 2004 (e and f). The delineated overlaid boxes define the regions where the simulated bloom occurs (box W) with the box further east (box E) capturing the winter bloom.

Streamlines of sea surface height (SSH; 0.1-m contours; white lines) in Figures 1a and 1b are used as a proxy for geostrophic mean ocean circulation. SWIO adequately resolves the main circulation pattern in the vicinity of the bloom, with the SEMC flowing poleward along the eastern coast of Madagascar, before rounding the southern Madagascan coast towards the Agulhas Current (Figures 1a and 1b). The eastward surface flowing SICC is also distinguished offshore of the SEMC (Menezes et al., 2014; Palastanga et al., 2007; Siedler et al., 2006), between 23°S and 27°S. Yet, this feature is shifted slightly north in the simulation (Figure 1b), a bias also present in the boundary forcings (GLORYS2V3-FREE) and in Lambert et al. (2016), hence potentially influencing the dynamics around the bloom. The vertical structure of simulated Chl-a shows high concentration within the first 50 m close to the coast, with a pronounced deep chlorophyll maximum (DCM) signal extending eastward at around 80–100 m (Figure 1c). This structure agrees well with Srokosz and Quartly (2013) who, from hydrographic data, observed a DCM at around 80- to 100-m depth along 47°–51°E in February 2005 (see Figure 3e of Srokosz & Quartly, 2013).

Across the zonal transect, the main features of simulated NO_3 in the upper 200 m are as expected, with high concentration close to the coasts due to coastal upwelling and decreasing concentration offshore (Figure 1e). Nonetheless, enhanced simulated NO_3 particles are found closer to the surface near the continental slope, a signature missing in CARS09 possibly due to the coarser spatial resolution. CARS09 also exhibits slightly higher patches of NO_3 in the upper 25 m but with a marginally deeper nutricline (>1 μmol/L). Generally, the similarities between observations and SWIO indicate a convergence of results, suggesting confidence in the model.

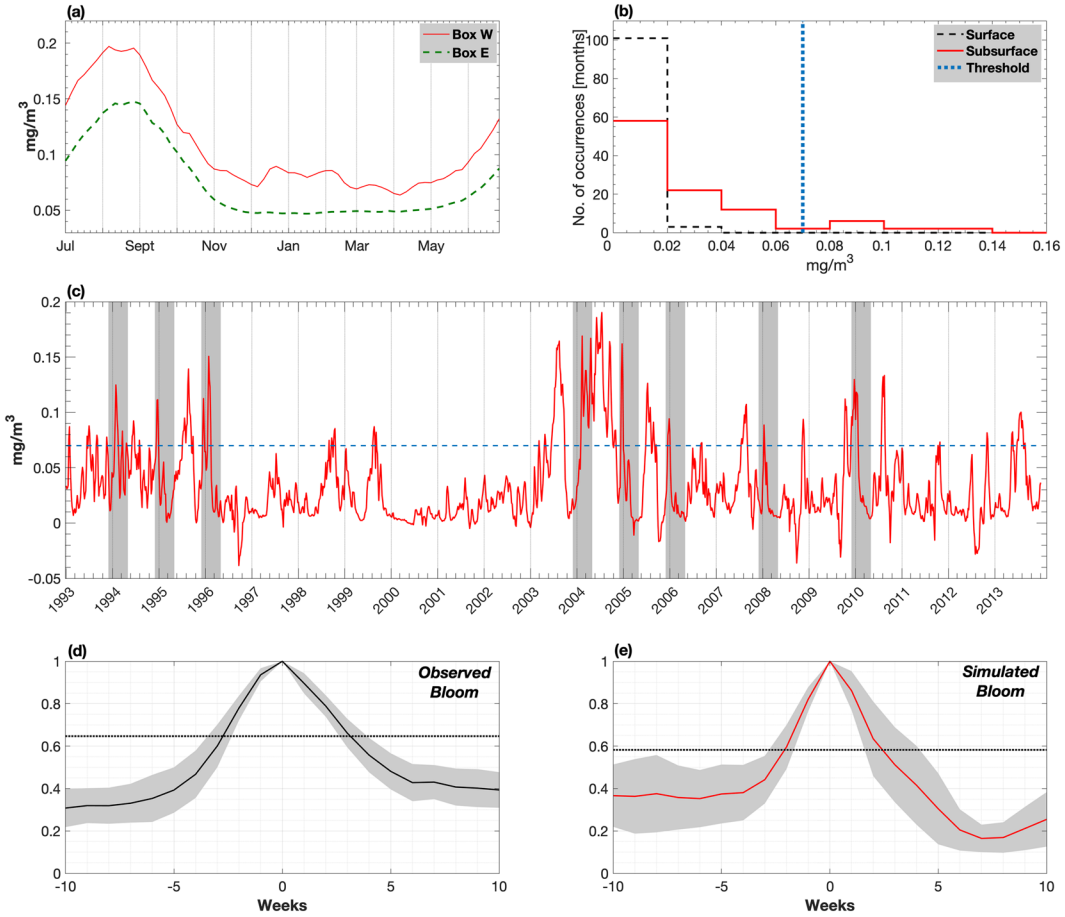

Figure 3. (a) Mean monthly climatology of simulated subsurface Chl-a concentration (mg/m^3) within box W (red line) and box E (green dashed line). (b) Histogram of occurrences of maximum monthly differences in Chl-a between box W and box E, in the surface (dashed black) and subsurface (full red) layers. (c) Bloom index computed by subtracting Chl-a of box E from box W. In (b) and (c), the blue dotted line indicates the 0.07 mg/m^3 threshold, and in (c), the gray shadings indicate identified simulated bloom years. Mean temporal composites of the observed and simulated bloom are shown in (d) (as in Dilmahamod et al., 2019) and (e), respectively. In (d) and (e), the gray shading envelopes the standard error at 95% confidence level, with the dotted horizontal black line indicating the mean of the maximum and minimum value of the composite, from which the duration of the bloom, in weeks, is obtained.

3. Simulated South-East Madagascar Bloom

The ability of SWIO to represent the South-East Madagascar Bloom is diagnosed, prior to the analysis of the processes involved. Exploring snapshots of surface Chl-a concentration (0–20 m; optical depth) revealed limited productivity in the bloom region (Figures 2a, 2c, and 2e).

Three distinct events, namely, January 1996, February 2004 and December 2004 (austral summer month of 2005), were characterized by a slight increase in surface Chl-a, but concurrently with a stronger increase within the 20- to 40-m layers (Figures 2b, 2d, and f). Inspecting Chl-a within the subsurface levels (20–40 m) for the 1993–2013 time period unveiled other similar pronounced signals. On this basis, a further investigation of this simulated subsurface bloom is performed. SWIO presents an austral summer phytoplankton bloom, a feature which is more significant in the subsurface layers (20–40 m) compared with the surface ones (0–20 m). For the three cases (January 1996, February 2004, and December 2004), a zonal extension of high Chl-a patches is observed south-east of Madagascar, with this band extending to 56°E in January 1996 and February 2004 (Figures 2b and 2d) and 58°E in December 2004 (Figure 2f). Note that these three events represent the strongest blooms throughout the available time-series (see Figure 3c).

Table 1
Summary of Identified Simulated Bloom Years, With the Corresponding Month at Which the Bloom Peaks

Bloom years	Month of maximum bloom
1994	January - 1994
1995	December - 1994
1996	January - 1996
2004	February - 2004
2005	December - 2004
2006	December - 2005
2008	January - 2008
2010	December - 2009

3.1. Identification of Simulated Bloom/non-bloom Years

The identification of simulated bloom and non-bloom events is achieved through a "model bloom index." Following the analysis of Dilmahamod et al. (2019), this bloom index consists of subtracting the Chl-a concentration in a box further offshore by a similar-sized box within the austral summer bloom patches. This allows for the filtering of the seasonal cycle, with only summer Chl-a peaks persisting. However, as stated previously, an over-estimation of simulated phytoplankton concentration is observed in the region during austral winter. This enhanced, coastally-confined Chl-a would consequently influence the computation of the bloom index, hence hindering the removal of the seasonal cycle. To overcome this non-homogeneity of austral winter's surface Chl-a in the Madagascar Basin, a bloom box (box W; 51°E–56°E, 22°S–28°S) is defined away from the high coastal winter bloom as much as possible, but within the austral summer bloom. A box further east (box E; 58°E–63°E, 22° S-28° S) is set close to box W, to capture a similar austral winter bloom intensity as box W, but not the austral summer bloom. From these two boxes (Figures 2a–2f), a model bloom index is defined.

The winter signal in box W is ~0.05 mg/m^3 stronger than in box E (Figure 3a), indicating a non-complete filtering of the seasonal cycle when computing the bloom index. However, within box W, a slight increase in Chl-a is observed as from early December, peaking at the end of December to early January, and eventually dissipating towards April (red line in Figure 3a). This signal is not present in box E and therefore provides confidence in the choice of the location of box W in representing the simulated austral summer bloom. To differentiate between bloom and non-bloom years, a bloom threshold is defined. Owing to the Chl-a concentration starting to increase as early as December (Figure 3a), a focus is put on the December–April time frame, from which a histogram of the number of occurrences of monthly maximum Chl-a difference (box W - box E) is built (Figure 3b) for the surface and subsurface levels, from 1993 to 2013. No crest is observed in the histogram for surface levels (black dashed line in Figure 3b), indicative of no bloom events. From the subsurface perspective, a trough is perceived between the 0.06–0.08 mg/m^3 range, from which the occurrences increased again between the 0.08–0.1 mg/m^3 range. Hence, a bloom threshold of 0.07 mg/m^3 (blue dotted line in Figure 3b) is assigned, with an exceedance of this threshold separating bloom and non-bloom occurrences. This threshold is consistent with the one used by Dilmahamod et al. (2019), which is based on satellite observations.

Figure 3c displays the model bloom index computed from box W and box E, overlaid with the 0.07 mg/m^3 threshold (blue dotted line). While most of the peaks exceeding the threshold are simulated winter blooms, the identified summer ones are distinguished by the gray shadings. Henceforth, unless stated otherwise, a South-East Madagascar (summer) Bloom entails enhanced Chl-a concentration averaged between the December of the previous year and April of the actual year. The study will also focus only on subsurface levels (20–40 m), with an occurrence of a phytoplankton bloom designating a bloom within these layers. From the mean temporal composite, the average duration of the simulated bloom is ~4–5 weeks (Figure 3e), compared with the 6 weeks of the observed bloom (Figure 3d; Dilmahamod et al., 2019), with the simulated one also dissipating more slowly than its development time (Figure 3e).

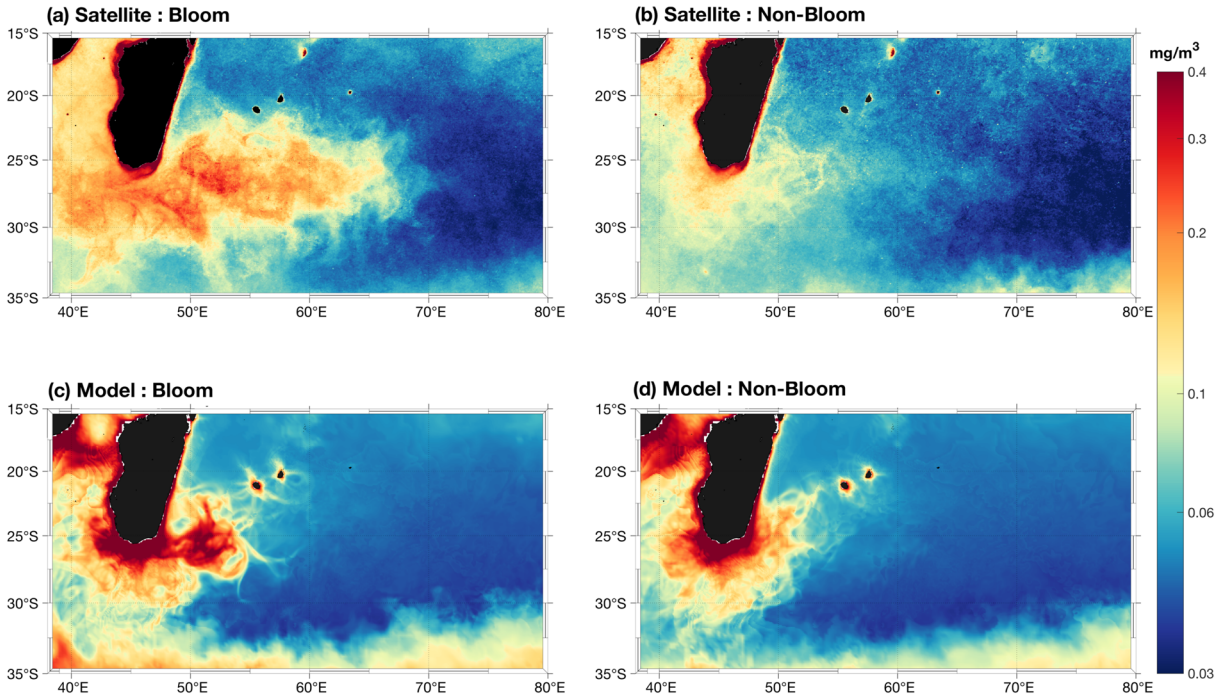

Figure 4. Composites of (a and c) bloom and (b and d) non-bloom events from (first row) remotely-sensed ocean color data set and (second row) SWIO. Bloom events in SWIO are identified in Figure 3. non-bloom events in both SWIO and satellite are Januaries of non-bloom years.

3.2. Temporal Variability

From a first glance at Figure 3c, the sporadicity trait of the bloom events observed in the ocean color data set is also present in the model. Eight years, namely, 1994, 1995, 1996, 2004, 2005, 2006, 2008, and 2010, are identified as bloom years in the model, with their initiation and termination, as well as the timing of the peaks varying significantly on temporal scales. Three out of these 8 years correspond to observed bloom years (2004, 2006, and 2008). Surprisingly, only two out of the three observed major bloom events (2004 and 2006; Dilmahamod et al., 2019) are reproduced by the simulation, with the strongest one (1999) not exceeding the bloom threshold in the model. Half of the ascribed simulated bloom years initiated early December and peaked at the end of December (1995, 2005, 2006, 2010), with three events (1994, 1996, and 2008) peaking in January. Interestingly, the 2004 event has one peak in February and a secondary peak in early April (Figure 3c). The stronger events occurred in 1996, 2004, and 2005 with peaks of approximately 0.2 mg/m^3. The details of bloom-occurrences are summarized in Table 1.

3.3. Horizontal Structure

The South-East Madagascar Bloom has been shown to exhibit large variability in terms of its meridional and zonal extent, besides its temporal one. The months with maximum phytoplankton concentration during bloom events and the Januaries of non-bloom years are merged to build Chl-a composites of bloom and non-bloom events. These are compared with the mean bloom and non-bloom periods over the satellite era (Figure 4). The mean spatial structure of the simulated bloom reveals higher productivity near the Madagascan coast (Figure 4c). This high patch of Chl-a extends from the coast up to 55°E, with a mean concentration exceeding 0.3 mg/m^3. However, the zonal extent of the simulated bloom is underestimated, with a branch of high Chl-a reaching 60°E (Figure 4c), whereas in satellite data, it extends up to 70°E (Figure 4a). Its meridional extent is observed between 22°S and 28°S (Figure 4c) compared with 22°–32°S in satellite (Figure 4a). During non-bloom years, some patches of enhanced Chl-a are still observed in the bloom region, with concentrations of ~0.15 mg/m^3, similar to ocean color data. The near-coastal Chl-a concentration remains, however, over-estimated.

3.4. Mean Vertical Physical Properties

The mean thermohaline structure of the water column associated with high and low Chl-a concentration in the bloom box is investigated. The bloom threshold used to identify bloom years, namely, 0.07 mg/m^3, is

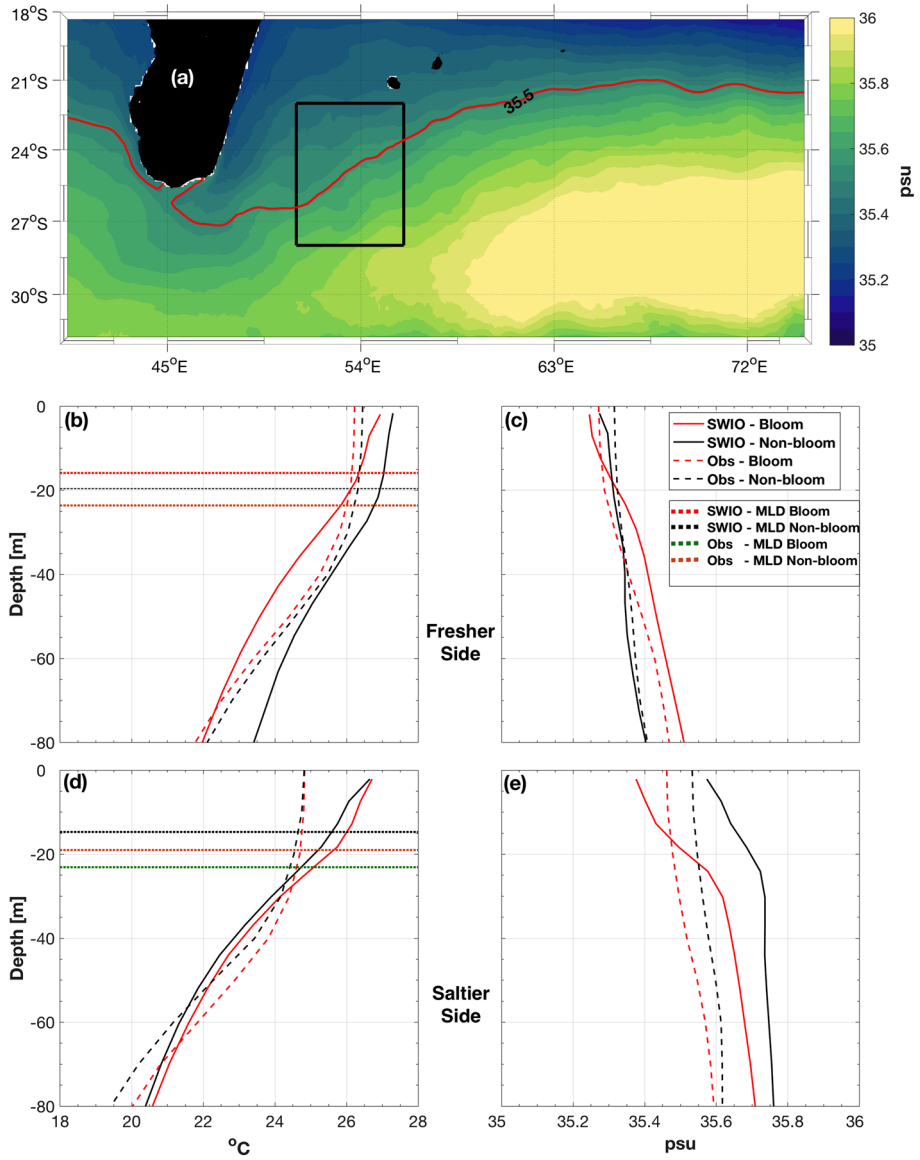

Figure 5. (a) Mean model salinity in the upper 20–40 m deep layers, averaged over austral summer (December–April) from 1993 to 2013. The red line indicates the 35.5 isohaline salinity front, used to separate the bloom region into a fresher (equatorward) and saltier (poleward) side. The black box delineates the bloom box. (b–e) Mean vertical thermohaline structure of the water column (temperature on left and salinity on right) within the simulated (full lines) and observed (dashed lines; as in Dilmahamod et al., 2019) bloom (red line) and non-bloom (black) patches, on the fresher (upper panels) and saltier (lower panels) side of the salinity front. The red (black) dotted lines indicate the simulated mixed layer depth during bloom (non-bloom), whereas the green (orange) dotted lines show the observed mixed layer depth during bloom (non-bloom) events.

employed to pinpoint spots of high Chl-a, with concentrations lower than 0.06 mg/m^3 designating no-bloom spots. This is performed during the time-step when the specific bloom is at its maximum. Henceforth, the mean vertical profiles related to bloom and non-bloom patches are referred to as "bloom profiles" and "non-bloom profiles," respectively. However, it should be noted that the bloom region exhibits a salinity front, assumed to be associated with the SICC (Menezes et al., 2014; Palastanga et al., 2007), that could hinder the inspection of the vertical haline structure. As in Dilmahamod et al. (2019), the analysis will focus on a fresher and saltier side of this aforementioned front, to prevent any bias. The 35.5 salinity contour is a valid isohaline as it separates the bloom box appropriately, into a fresher and saltier side. In Figure 5a, the low-salinity signature close to the Madagascan coasts is representative of the fresher poleward-flowing SEMC.

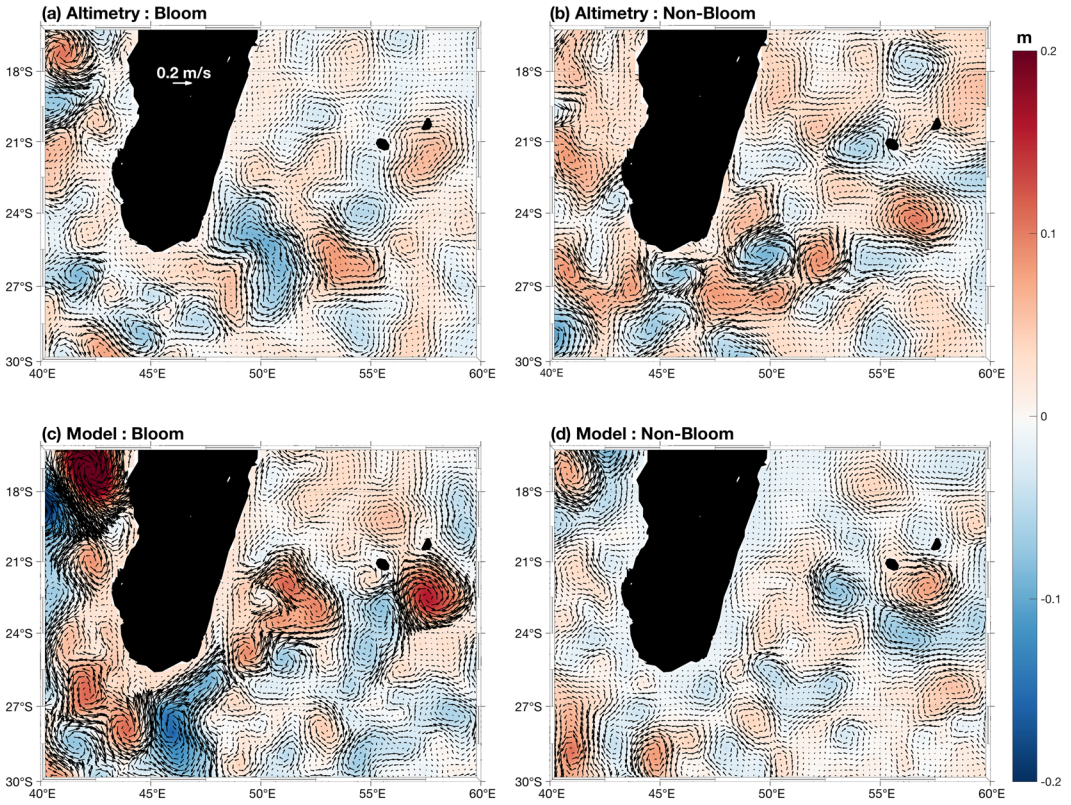

Figure 6. Comparison of sea level anomalies (m) overlaid with surface geostrophic velocity anomalies (m/s) from (upper row) altimetry and (lower row) the model, for (left panel) bloom and (right panel) non-bloom period. For each bloom event, 2 weeks prior to the first exceedance of the 0.07 mg/m^3 threshold, and for each non-bloom event, 2 weeks prior to the maximum austral summer Chl-a concentration, are collated to build the composites. Note that in both observation and model data, the 2004 bloom event is not considered, owing to this specific event being likely triggered by tropical cyclonic activity (Dilmahamod et al., 2019).

The vertical structure of the water column for observed bloom/non-bloom patches is also plotted in Figures 5b–5e, as in Figure 6 from Dilmahamod et al. (2019). Generally, the main thermocline characteristics from the observations are well reproduced in SWIO, except for a slight deviation in intensities. As in observations, it is revealed that simulated bloom occurrences coincide with a shallow stratified mixed layer on both sides of the front (Figures 5b and 5d). On the fresher side, the mean temperature within high Chl-a patches is ~1°C lower than non-bloom profiles, except in the upper layers (Figure 5b), hence indicating a possible intrusion of colder and nutrient-rich waters from the subsurface levels. This intrusion of subsurface waters is also reflected in the shallower mixed layer depth (red dotted line: ~15.9 m) during bloom compared with non-bloom patches (black dotted line: ~19.7 m). However, these remain shallower compared with observed bloom and non-bloom mixed layer (both at ~23.6 m in Dilmahamod et al., 2019; orange dotted line). On the saltier side (poleward side), bloom profiles exhibits slightly higher temperature compared with non-bloom profiles. The simulated mixed layer depth (black dotted line) is similar for both high and low Chl-a patches, but shallower than in observations (dotted green and orange for bloom and non-bloom respectively; Figure 5d). Overall, the mixed layer sits at a relatively shallow depth within the bloom region.

The vertical haline structure of both fresher and saltier sides of the front reveals a low-salinity signature in the surface levels, associated with bloom profiles (Figures 5c and 5e). This is the case for the upper 20 m only, on the fresher side (Figure 5c), whereas the low-salinity water persists deeper than 80 m on the saltier side, for which the difference in the upper 20 m is ~0.2 psu (Figure 5e). This low-salinity signature could have various sources, including (i) advection of fresher SEMC coastal waters, (ii) upwelling of fresher deeper waters, or on a smaller scale, (iii) the input of freshwater at the surface from enhanced rainfall.

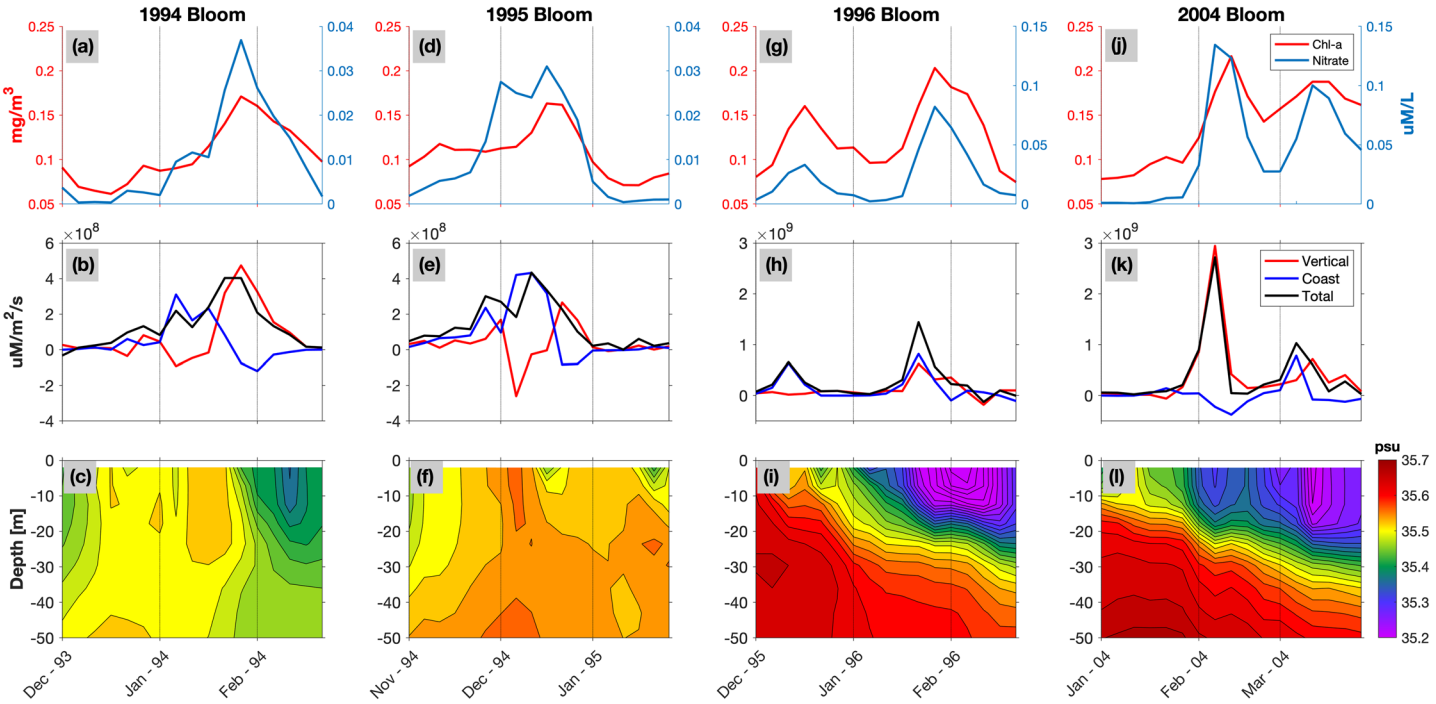

Figure 7. The time series of mean simulated Chl-a (mg/m^3; red line) and NO_3 (μM/L; blue line) concentration, averaged between 20 and 40 m deep (upper row). Simulated NO_3 fluxes (μM/m^2/s) over the 20- to 40-m depth range, with the red and blue lines indicating flux from the subsurface (vertical) and Madagascan coast (advection from the west). The total flux (horizontal + vertical) is shown by the black line (middle row). Hovmöller of the mean vertical structure of salinity in the bloom box (bottom row). These are performed for specific bloom events, namely, the 1994 (first column), 1995 (second column), 1996 (third column), and 2004 (fourth column) bloom years. Please note the different *y* axis for NO_3 concentration (first row) and NO_3 fluxes (second row) during the distinct events.

In summary, the South-East Madagascar Bloom is observed in the high-resolution coupled model (SWIO), as a subsurface bloom concentrated within the 20- to 40-m depth range. A bloom threshold of 0.07 mg/m^3, similar to the one used from ocean color data set (Dilmahamod et al., 2019), is applied to distinguish simulated bloom and non-bloom events, yielding eight bloom events. These exhibit large temporal variability, with 50% initiating and peaking in December of the previous year. The remaining events peak in January while the 2004 one peaks in February. Spatially, the simulated bloom does not spread zonally as the observed bloom, but it is more highly concentrated close to the coast. Interestingly, the simulated bloom occurs within a shallow-stratified layer, with a low-salinity signature within the surface layers, as reported by Dilmahamod et al. (2019), which is based on a co-location of Argo floats and satellite Chl-a data.

While SWIO is able to reproduce a phytoplankton bloom with some similar characteristics as the observed one, it should be noted that the version of PISCES used here does not include some processes which could potentially be important in resolving the complete picture of the South-East Madagascar phytoplankton bloom. These include the non-parameterization of nitrogen-fixers, shown to be the dominant species in the region during the bloom (Srokosz & Quartly, 2013; Poulton et al., 2009), as well as the representation of river runoffs which could likely inject enhanced nutrient-rich waters in the surface waters along the Madagascan coast. The representation of river runoffs, as well as explicitly resolving nitrogen-fixing cyanobacteria, could provide a geochemical niche favorable for N_2-fixation within the surface layers. Hence, the discrepancies associated with the presence of enhanced Chl-a concentration in the subsurface instead of the surface layers and a reduced zonal extension of the simulated bloom might be better represented within an updated biogeochemical modeling component. Nonetheless, the large temporal and spatial variability of the subsurface bloom, being confined within a shallow stratified layer with low-salinity signature at the surface, still highlights some similarities in potential processes associated with the simulated and observed bloom, allowing confidence in a more detailed analysis of the model result.

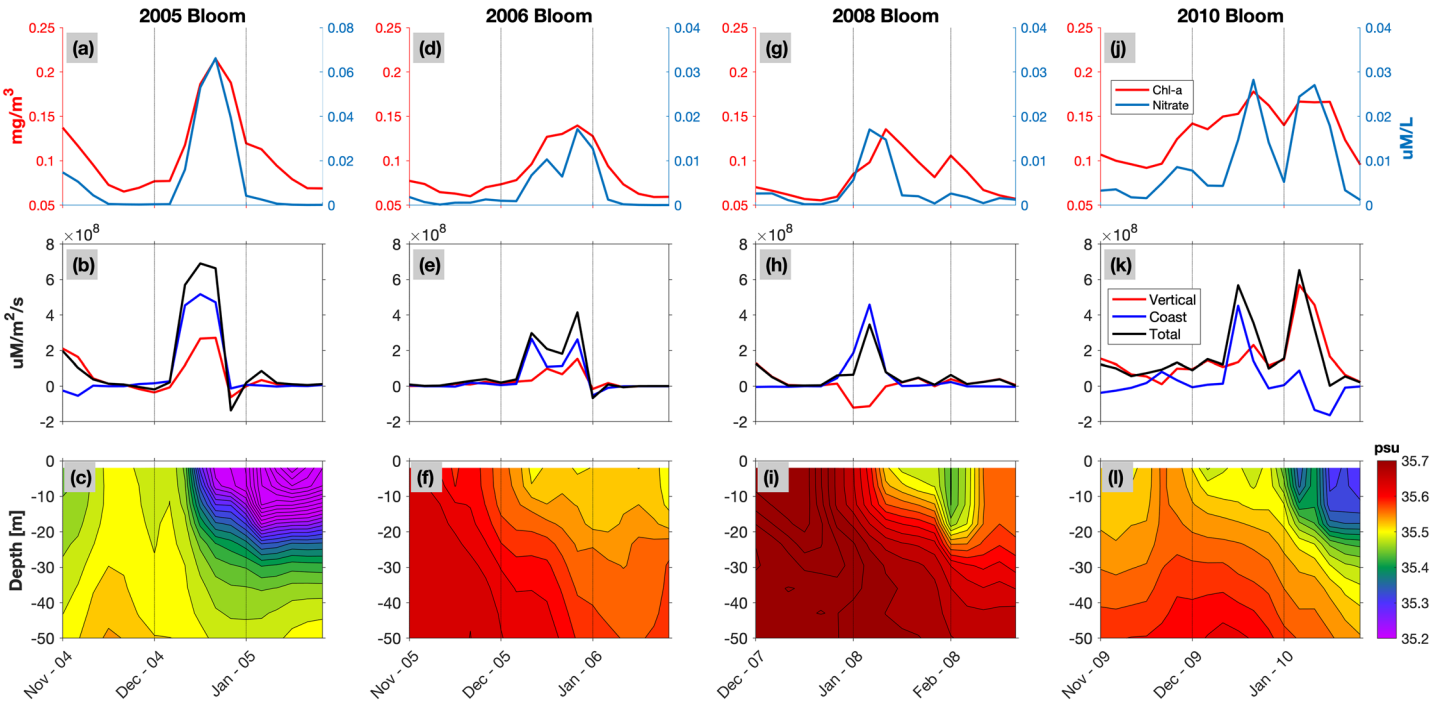

Figure 8. Similar to Figure 7, but for the 2005 (first column), 2006 (second column), 2008 (third column), and 2010 (fourth column) bloom years.

4. Advection of SEMC Waters

4.1. Local Circulation Associated with the bloom

The oceanic flow associated with bloom and non-bloom events is analyzed using both altimetry and the model data. To present only the local fluctuations of the circulation (Figure 6), the regional monthly climatology calculated over the 1998–2016 (1993–2013) time period for the altimetry (model) is subtracted. Contrasting structures in the local circulation, associated with bloom and non-bloom events, are revealed. The flow south-east of Madagascar exhibits a dipole-like circulation, with an anticyclonic eddy centered at around 22.5° S–50°E, and a cyclonic one on its south, south-western flank at 24.5°S–49°E (Figure 6a). This dipole-like feature is also perceived, but further south, in the model (Figure 6c), with an anticyclonic eddy at 25°S–49°E and cyclonic eddy at 26° S-48° E. Assessment of individual bloom periods (not shown here) affirmed that the dipole-like feature occurred repeatedly and was not simply an artifact of one strong feature in the time period aliasing the composite. The existence of this dipole circulation during bloom events leads to an offshore detachment of the SEMC, advecting water eastward and possibly feeding the eastward surface flowing SICC. It causes a disruption of the mean flow further downstream, where the south-westward flow is reduced (Figures 6a and 6b). On the other hand, during non-bloom years, this particular characteristic of the mean flow is absent (Figures 6b and 6d). An anticyclonic circulation can be observed in altimetry data, centered at 24°S–49°E (Figure 6b), which seems to strengthen the coastal south-westward flow. In SWIO, there is very little eddy-mean flow interaction (Figure 6d), and hence, the SEMC remained undisturbed by eddy activity in the region. Consequently, no retroflection was observed in the vicinity during non-bloom events.

4.2. Simulated Nutrient Flux Analysis

The dipole-like circulation south-east of Madagascar and subsequent detachment of the SEMC during bloom years may influence the biogeochemical dynamics of the region. Enhanced productivity is observed on the south-eastern Madagascan coast (see Figures 2, S1, and S2 in Voldsund et al., 2017), indicating nutrient-rich SEMC waters. Horizontal advection of this fresher nutrient-rich SEMC waters in the bloom vicinity, or vertical fluxes of nutrients and/or phytoplankton biomass from the subsurface layers, as a result of Ekman suction, can trigger enhanced productivity. Hence, the response of upwelling intensity and nutrients input from the Madagascan coast are investigated through a nitrate (NO_3) flux analysis (Figures 7 and 8). This is performed within the "model bloom box" and within the 20- to 40-m depth range. From a biogeochemical

context, a net positive incoming flux from the Madagascan coast would be indicative of coastal nutrients input in the bloom box, whereas a net positive vertical flux would enhance the amount of nutrient supply due to upwelling. In line with a possible intrusion of fresher waters from the Madagascan coast, the subsurface layers or less significantly heavy rainfall, the mean vertical structure of salinity is also explored. This analysis is performed separately, as case events for each simulated bloom year.

Bloom events of 1994 (January) and 1995 (December 1994) revealed quite similar processes. Chl-a concentration increased concurrently with an intensifying positive flux of NO_3 from the Madagascan coast (blue line in Figures 7b and 7e). As input from the coasts is reduced, the nutrient supply from vertical fluxes (upwelling) increases (red line in Figures 7b and 7e), with the mean Chl-a concentration peaking at the same time as the vertical flux and NO_3 concentration (Figures 7a and 7d). Thus, the 1994 and 1995 simulated blooms events are triggered by horizontal advection of nutrients from the coasts and ultimately sustained through upwelling. Nonetheless, the 1994 bloom appears to be controlled mostly by vertical fluxes, which are more intense during the bloom peak. An opposite effect in salinity is observed during that year, with enhanced coastal (vertical) fluxes inducing a slight increase (decrease) in salinity (Figure 7c). This intrusion of low-salinity water is less evident during the 1995 event, with a slight reduction in salinity mid-December 1994 (Figure 7f).

The 1996 bloom event, one of the strongest events, was characterized by two Chl-a peaks, with the first one in mid-December 1995 and a more intense secondary peak end of January 1996. The first peak occurred simultaneously with an enhanced NO_3 flux from the coast (Figure 7h) and an intrusion of lower-salinity water (Figure 7i). The more intense secondary Chl-a peak seemed to respond to nutrients supply from both the Madagascan coast and upwelling, although the flux is slightly more significant from the coasts (Figure 7h). These incoming fluxes are accompanied by a low-salinity signature in the water mass (Figure 7i).

The strongest simulated bloom event occurred in 2004, reaching a concentration of ~0.22 mg/m^3 (Figure 7j). NO_3 flux into the bloom region was dominated by vertical fluxes only (Figure 7k), indicating strong upwelling, rather than horizontal advection playing a role in nutrient supply. A secondary peak of this bloom appeared in mid-March 2004 due to horizontal advection of NO_3 from the coasts, together with NO_3 from the subsurface levels (Figure 7k). Similar to the 1996 event, the positive vertical flux concurs with an intrusion of low-salinity water in the region (Figure 7l). Both the 1996 and 2004 events were characterized by a higher concentration of nitrate as well as nitrate fluxes (Figures 7g and 7h for 1996; Figures 7j and 7k for 2004), compared with the previous bloom years. This is also reflected in the lower-salinity signature in those 2 years and could potentially be related to different processes and/or water masses influencing the bloom region.

The 2005 and 2006 bloom events peaked towards the end of December of the previous year (2004 and 2005, respectively; Figures 8a and 8d). The productivity is controlled by the high NO_3 concentration which occurs at the same time. In these two case events, the NO_3 fluxes are dominated by horizontal advection from the Madagascan coast, indicative of high-nutrient waters from the eutrophic coastal regions. However, these also occur simultaneously with a slight increase in upwelling intensity (Figures 8b and 8e). As expected, the eastward inflow of nutrients is also evident through the low-salinity signature (Figures 8c and 8f), representative of coastal SEMC water being advected into the bloom region. Nonetheless, the contrast in the concentration of fresher waters between these two bloom periods is evident and revealed different water mass characteristics with distinct possible circulation patterns, at play in reducing the surface salinity.

In late 2007, the south-east Madagascar region is quite oligotrophic until a peak of NO_3 flux from the coasts (Figure 8h) initiates a bloom which peaks early January 2008 (Figure 8g). The enhanced productivity is induced through horizontal NO_3 advection only, as the vertical flux is dampened at the same time. Comparable with previous bloom events (1996, 2005, and 2006), the intrusion of low-salinity water coincides with the increase in advection flux from the coasts (Figure 8i). The 2010 bloom is sustained for almost 1 month, with high productivity starting from mid-December 2009 to 23rd January 2010 (Figure 8j). This is due to a contribution of nutrients from both the Madagascan coast, which peaks mid-December 2009, and from the subsurface levels beneath the bloom, peaking early January 2010 (Figure 8k). Hence, horizontal advection from the coast contributes to the onset of the bloom, with vertical input bringing nutrients to sustain it for a longer time. Both fluxes from the west and subsurface levels are associated with a decreased salinity in the bloom region (Figure 8l), although the strongest salinity decrease was as a result of vertical input.

Table 2
Summary of Which Bloom event is Dominated by Incoming Eastward Fluxes or Vertical Fluxes of NO_3

Bloom years	Vertical NO_3 flux	NO_3 flux from Madagascan coast
1994	X	
1995		X
1996		X
2004	X	
2005		X
2006		X
2008		X
2010		X

Table 2 provides a summary of the dominant fluxes, either horizontal flux from the Madagascan coast or vertical flux from the subsurface layers associated with each bloom events. The 1994 and 2004 bloom years were mostly influenced by the vertical fluxes of NO_3. For the remaining six events, the input of NO_3 through the western boundary of the model bloom box controlled the productivity in the region, although upwelling of nutrient-rich waters from the deeper layers could still play a minor role. The intrusion of coastal waters as well as deeper waters in the bloom region is also identified by a lower-salinity signature within the first 40 m of the water column. Thus, low-salinity and nutrient-rich waters representative of the coastal SEMC can be advected into the bloom region through the dipole-like feature in the local circulation, hence contributing to the initiation of a phytoplankton bloom.

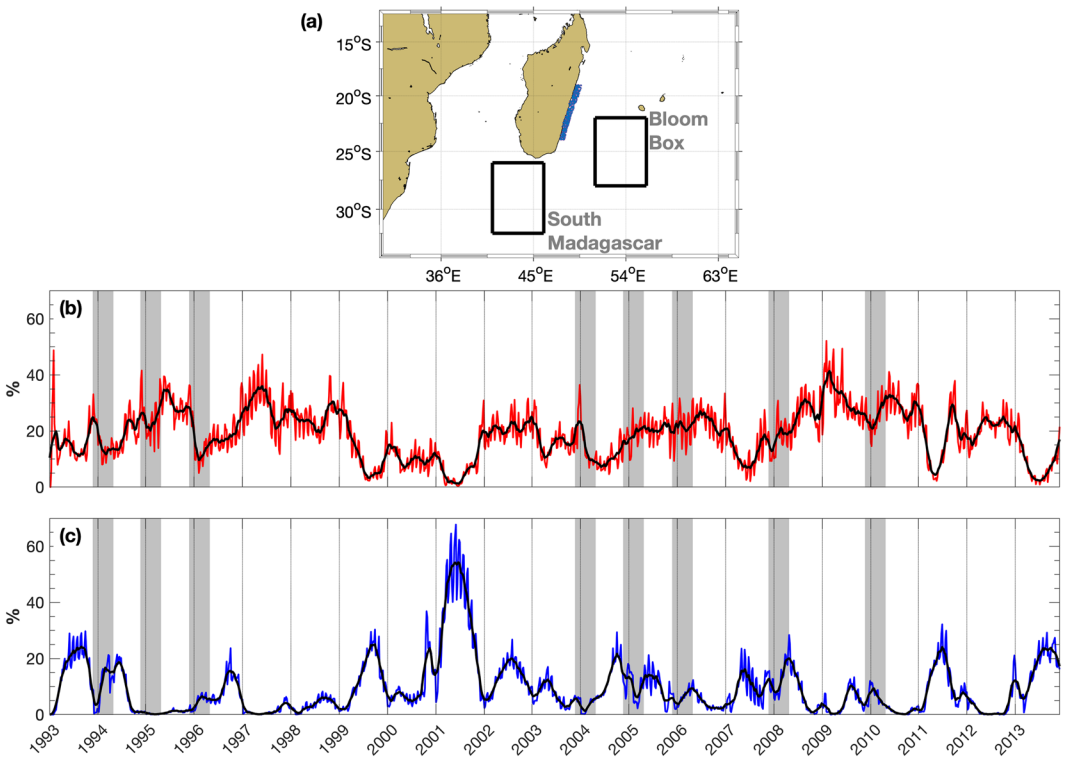

Figure 9. (a) The release area of 500 particles (in blue) per month, as represented in the model. The two delineated boxes indicate the region through which the Lagrangian particles are tracked. (b and c) Time series of the percentage of particles arriving in the (b) bloom box and (c) south of Madagascar. The black line in (b) and (c) is the 1-month running mean of the specific time series. The gray shadings indicate identified simulated bloom years.

4.3. Lagrangian Particle Tracking

The possible advection of low-salinity, nutrient-rich SEMC waters into the bloom region is explored using the Lagrangian transport model, Ichthyop (Lett et al., 2008), in combination with the high-resolution SWIO configuration. Ichthyop is a model developed to study the effects of physical and biological factors on marine particles (Lett et al., 2008). Five hundred particles were released, every month, in the surface layers of the SEMC (Figure 8a), with each of them having a lifetime of 90 days, after which they are assumed "dead." Ninety days is considered sufficient time for the particles to reach either the "bloom box" or the box south of Madagascar (Figure 9a), as shown by Srokosz et al. (2015). This experiment is repeated monthly from 1993 until 2013, and the percentages of particles reaching the bloom box and south of Madagascar are assessed. A higher percentage of particles in the bloom region would be representative of advection of coastal waters which could fertilize the South-East Madagascar Bloom.

Unsurprisingly, the Lagrangian particles released in the coastal SEMC were observed to be advected offshore towards the south-east Madagascar region. During the first three events, namely, 1994, 1995, and 1996, the percentage of particles in the bloom area peaked prior to the event, at 32%, 42%, and 37%, respectively (Figure 9b). Simultaneously, the box south of Madagascar exhibited a lower number of particles (Figure 9c). Yet, among these three events, 1994 displayed a smaller percentage of particles (32%) and is a year which was mostly characterized by a dominant input of NO_3 from the subsurface levels (Figure 7b). The 2004 bloom, also dominated by upwelling processes, displayed a peak in particles early January (36%), although this did not have an apparent influence on the input of NO_3 (Figure 7k) in the bloom box. The four remaining bloom years had approximately 30% of particles transported into the bloom region except during 2005 where only 21% were accounted for. This could still be representative of coastal SEMC waters moved offshore. An important note is that an increase in particles in the bloom box co-occurred mostly with a decrease south of Madagascar and vice versa (Figure 9c). Nonetheless, some non-bloom years also presented high percentages of particles such as in 1993 (47%), 1999 (37%), and 2009 (52%). Additionally, a similar analysis using the coarser altimetry data was conducted (not shown here). An intermittency in the number of particles advected in the bloom vicinity was observed, with some peaks during bloom years.

5. Discussion

Dilmahamod et al. (2019) proposed a new hypothesis that could explain the distinct biological feature of the South-West Indian Ocean, namely, the South-East Madagascar Bloom. This hypothesis entails the detachment of a stronger than usual SEMC from the coasts, hence advecting nutrient-rich and low-salinity waters in the Madagascar Basin, triggering the bloom. This hypothesis is investigated using a high-resolution coupled biophysical model (SWIO), based on CROCO and PISCES. This configuration performs a fairly good job in adequately resolving the mean physical properties in the region, although the position of the SICC is shifted slightly north. This northward shift is, however, also apparent in a high-resolution modeling study in the South Indian Ocean (Lambert et al., 2016), as well as the boundary forcings of the configuration used. From a biogeochemical perspective, coastal Chl-a around southern Madagascar is slightly over-estimated. Nonetheless, no austral summer bloom is observed in the upper layers (0–20 m; optical depth), but a subsurface (20–40 m) bloom appears sporadically. Previous studies revealed the presence of enhanced subsurface Chl-a in the region (Srokosz & Quartly, 2013). Spatially, this subsurface bloom displays a similar filamentous structure as described by Longhurst (2001). The inconsistencies between the observed and simulated bloom could, however, be related to the configuration, which does not incorporate river discharges as well as the parameterization of the dominant nitrogen-fixing cyanobacteria (Srokosz & Quartly, 2013; Poulton et al., 2009). Nonetheless, the subsurface bloom and its irregular enhancement deserve to be explored.

A similar identification method, as in Dilmahamod et al. (2019), was employed to distinguish bloom and non-bloom years. An index was computed from which an exceedance of a specific threshold would be distinguished as a simulated bloom year. A 0.07 mg/m^3 threshold was obtained, in agreement with Dilmahamod et al. (2019). The simulated bloom displayed substantial temporal variability. In total, eight bloom years were identified (1994, 1995, 1996, 2004, 2005, 2006, 2008, and 2010), with 2004, 2006, and 2008 also identified as bloom years in observations (Dilmahamod et al., 2019; Raj et al., 2010; Uz, 2007). The model only reproduced two (2006 and 2008) of the three major bloom events and did not capture the strongest 1999 one (Dilmahamod et al., 2019). The inability of the simulation to reproduce all the observed bloom years

possibly indicates a signature of the turbulent and chaotic processes associated with a bloom appearance. The years 1996, 2004, and 2005 were the strongest events, with Chl-a concentration exceeding 0.2 mg/m^3. The peak month varied significantly, with some peaking in December (1995, 2005, 2006, and 2010), January (1994, 1996 and 2008), and February (2004). On spatial scales, the simulated bloom also displays large variability, as observed in satellite data (Dilmahamod et al., 2019; Uz, 2007; Wilson & Qiu, 2008). Comparable with observations, the simulated bloom occurred within a mean latitudinal band of 22°S–28°S (22°S–32°S in observations), but its zonal extent is under-estimated, reaching ~60°E (70°E in observations; Dilmahamod et al., 2019). Interestingly, as concluded in previous studies (Dilmahamod et al., 2019; Srokosz & Quartly, 2013; Uz, 2007), the simulated bloom occurred within a shallow-stratified mixed layer, with low-salinity signature at the surface. Thus, similar processes may be at play in both the simulated and observed bloom.

The mean local circulation associated with bloom and non-bloom years displayed a heterogeneous structure, with a dipole-like feature present south-east of Madagascar during bloom years. This anticyclonic and cyclonic eddy-like circulation favored an early detachment of the SEMC, pushing coastal waters eastward in the Madagascar Basin. This fate of the SEMC where a partial retroflection of the flow is observed has been shown in previous studies (Halo et al., 2014; Siedler et al., 2009) and could possibly be associated with the local effect of mesoscale eddies, namely, the South Indian Ocean eddies (Dilmahamod et al., 2018; Ponsoni et al., 2016). After rounding the southern tip of Madagascar, the south-westward flow is either increased or unchanged during non-bloom years, whereas a reduction or even reversal of the flow is noted during bloom years. Owing to the reduction/reversal of the flow, the current-driven upwelling south of Madagascar would be dampened during bloom years, in line with the findings of Dilmahamod et al. (2019). The coupled biophysical model simulates a sporadic (subsurface) phytoplankton bloom, associated with similar mean vertical properties within the water column and in a regime of local circulation which favors a lower intensity of the current-induced upwelling south of Madagascar (Dilmahamod et al., 2019). This allowed further investigation of the causes of this bloom.

An input of fresher waters in the bloom region, hence increased stratification, concurrently with an injection of nutrients can provide the right conditions for enhanced productivity. Thus, a NO_3 flux analysis was performed to investigate the two main sources of nutrients, including (i) vertical advection of nutrients from the subsurface through upwelling and (ii) horizontal advection of nutrient-rich SEMC waters from the Madagascan coast. However, local biogeochemical recycling could also result in an increase in nutrients in the upper layers of the water column (Zhang et al., 2016). Six out of eight bloom events were largely dominated by an injection of NO_3 from the Madagascan coast, also associated with a low-salinity signature, hence representative of fresher coastal SEMC waters. Advection of low-salinity, nutrient-rich waters from West Greenland also plays a role in the spring phytoplankton bloom in the Labrador Sea, thus showing an analogy of the physical drivers of the blooms (Frajka-Williams et al., 2009). Similar to the south-east Madagascar region, the Labrador Sea is influenced by strong eddies which impacted the separation of a boundary current (Frajka-Williams et al., 2009). Nonetheless, uplifting of low-salinity nutrient-rich subsurface waters from the deeper layers might also play a minor role in contributing to the net NO_3 flux during those years.

The other two events, namely, 1994 and 2004, were triggered and sustained only through vertical advection of NO_3. The model is able to reproduce the 2004 bloom, a year also defined as bloom year in observed dataset. Enhanced NO_3 concentration was sourced from the subsurface layers, an indication of upwelling processes at play. This is in agreement with Dilmahamod et al. (2019), who observed a highly positive peak in Ekman pumping during 2004, owing to a negative wind stress curl. This signature in both observational and simulated data resulted from cyclonic activities in the region. Two tropical cyclones were present during this period, with Elita (26th January to 5th February) ending its track in the bloom region and Gafilo (1st–18th March) passing close by early March. However, an inspection of cyclonic activities and the surface forcings revealed the absence of a tropical cyclone near the bloom region in 1994. Associated intense cyclonic winds can induce stirring and divergent geostrophic currents, resulting in a deepening of mixed layer depth and enhanced nutrients injected into the surface layers (Lin et al., 2003; Shi & Wang, 2007; Subrahmanyam et al., 2002). Thus, it can be concluded that when atmospherically forced, the SWIO configuration is able to reproduce a phytoplankton bloom. The local transient wind-driven upwelling can also influence vertical fluxes and hence increased phytoplankton biomass, as is observed on the continental shelf off Ningaloo Reef, north-western Australia in austral spring-summer (Zhang et al., 2016). Both Elita and Gafilo also made landfall, with high precipitation, over Madagascar, which could have contributed to an

additional supply of nutrients, from river runoffs, into SEMC coastal waters. However, the effect of river runoffs is not parameterized in the configuration and hence cannot be assessed.

The intrusion of low-salinity SEMC waters was further investigated using Lagrangian particles, where 500 particles were released every month in the SEMC and then tracked. Srokosz et al. (2015) demonstrated that particles from the SEMC can get advected offshore, hence fertilizing the bloom. The significant interannual variability associated with the number of particles in the bloom area illustrates the intermittent supply of nutrient-rich coastal waters, hence inducing the sporadic enhancement of Chl-a. High numbers of particles arrived in the bloom box during the first three bloom events (1994, 1995, and 1996), representative of an influx of low-salinity coastal SEMC waters, bringing nutrients and triggering a bloom. No significant peaks are observed during the other bloom months, but concomitantly, the number of particles south of Madagascar was relatively low. Similar analysis with altimetry showed large intermittency of the number of particles advected from the coasts to offshore, but the link with specific bloom years was not conclusive. Using a high-resolution model and a different Lagrangian particle model, Srokosz et al. (2015) concluded that iron particles, from coastal waters, could be advected eastward through the mesoscale eddy field, hence supporting the bloom the next year. They also showed the significant spatial variability in the dispersal of the particles which could explain the substantial interannual variability in the spatial extent of the observed bloom. Nonetheless, the analysis in this study provides evidence of the significant temporal variability which could control the sporadic aspect of the South-East Madagascar Bloom.

6. Summary

The possible influence of the coastal nutrient-rich SEMC waters on the sporadic South-East Madagascar Bloom is investigated using a high-resolution coupled biophysical model. This study is the first (to our knowledge) to model this biological phenomenon in the Madagascar Basin. The model is able to resolve an intermittent austral summer Chl-a enhancement, but in the subsurface levels (20–40 m). From 21 years of model data, eight bloom years were identified, with three bloom years (2004, 2006, and 2008) in agreement with ocean color data set. The model also exhibits large spatial and temporal variability, with high phytoplankton concentration confined within a shallow mixed layer with low-salinity surface waters. This is consistent with observations (Dilmahamod et al., 2019; Srokosz & Quartly, 2013; Uz, 2007) and indicates that possible similar mechanisms may be at play.

Dilmahamod et al. (2019) proposed a new hypothesis that could explain the triggering of the bloom, stating that the advection of fresher coastal nutrient-rich SEMC waters could increase the stratification in the Madagascar Basin, providing the right conditions for a cyanobacterial phytoplankton bloom. Although nitrogen fixers are not resolved in this configuration, a subsurface bloom is still present and hence provides a base for understanding the physical processes driving it in the model. It is shown that advection of this water mass concurrently occurs with the simulated SEMC, with its interannual variability driving the sporadic phytoplankton enhancement of the region. The southern SEMC appears to act as a gate allowing water to either flow towards the northern Agulhas Current or switching into a retroflection loop, diverting water into the Madagascar Basin. Such behavior is consistent with the description of Siedler et al. (2009) and might explain the controversy for the existence or not of a retroflection of the SEMC (Lutjeharms, 1981; Quartly & Srokosz, 2002).

It should be stressed that even though nitrogen-fixers are not essential to simulate a bloom, their non-parameterization could justify the spatial and temporal inconsistencies of the simulated bloom. Taking into account that the bloom occurs at boundaries of enhanced nitrogen fixation rate, namely, *Trichodesmium* occurrences (see Figure 11 in Wilson & Qiu, 2008), this could explain the absence of high phytoplankton concentration within the surface layers as well as the under-estimation of its eastward zonal extension. This study provides the first base for modeling the bloom in the future, and it is expected to help in designing further experiments, such as a configuration with the parameterization of nitrogen-fixers and including river discharges. It is also essential that the findings from this study are further supported by future observations, which should lead to a better understanding of this complex feature.

Acknowledgments
The authors would link to thank three anonymous reviewers for comments and suggestions that greatly improved this manuscript. Dilmahamod A. F. acknowledged funding from the National Research Foundation (NRF; grants 90270 and 98183), the International Centre for Education, Marine and Atmospheric Sciences over Africa (LMI ICEMASA), and the Institut de Recherche pour le Developpement (IRD). The financial assistance of the South African Environmental Observation Network (SAEON) towards this research is also acknowledged. Opinions expressed and conclusions arrived at are those of the author and are not necessarily to be attributed to SAEON. The modeling tools CROCO-PISCES were provided by IRD. The data from the simulations are available online at the Zenodo repository with https://doi.org/10.5281/zenodo.3770408 - Version 2 (Link: https://zenodo.org/record/3482920#.XqOdpXKRWpc)

References

Argo (2000). *Argo float data and metadata from Global Data Assemby Centre* (Argo GDAC). SEANOE. https://doi.org/10.17882/42182

Aumont, O., & Bopp, L. (2006). Globalizing results from ocean in situ iron fertilization studies. *Global Biogeochemical Cycles*, *20*, GB2017. https://doi.org/10.1029/2005GB002591

Böhme, L., & Send, U. (2005). Objective analyses of hydrographic data for referencing profiling float salinities in highly variable environments. *Deep Sea Research Part II*, *52*(3-4), 651–664. https://doi.org/10.1016/j.dsr2.2004.12.014

Berman-Frank, I., Cullen, J. T., Shaked, Y., Sherrell, R. M., & Falkowski, P. G. (2001). Iron availability, cellular iron quotas, and nitrogen fixation in Trichodesmium. *Limnology and Oceanography*, *46*(6), 1249–1260. https://doi.org/10.4319/lo.2001.46.6.1249

Capone, D., Zehr, J., Paerl, H., Bergman, B., & Carpenter, E. (1997). Trichodesmium, a globallly significant marine cyanobacterium. *Science*, *276*(MAY), 1221–1229.

Debreu, L., Marchesiello, P., Penven, P., & Cambon, G. (2012). Two-way nesting in split-explicit ocean models: Algorithms, implementation and validation. *Ocean Modelling*, *49-50*, 1–21. https://doi.org/10.1016/j.ocemod.2012.03.003

Dee, D. P., Uppala, S. M., Simmons, A. J., Berrisford, P., Poli, P., Kobayashi, S., et al. (2011). The ERA-Interim reanalysis: Configuration and performance of the data assimilation system. *Quarterly Journal of the Royal Meteorological Society*, *137*(656), 553–597. https://doi.org/10.1002/qj.828

Dilmahamod, A. F., Aguiar-González, B., Penven, P., Reason, C. J. C., De Ruijter, W. P. M., Malan, N., & Hermes, J. C. (2018). SIDDIES Corridor: A major east-west pathway of long-lived surface and subsurface eddies crossing the subtropical South Indian Ocean. *Journal of Geophysical Research: Oceans*, *123*, 5406–5425. https://doi.org/10.1029/2018JC013828

Dilmahamod, A. F., Penven, P., Aguiar Gonzalez, B., Reason, C. J. C., & Hermes, J. C. (2019). A new definition of the South-East Madagascar Bloom and analysis of its variability. *Journal of Geophysical Research: Oceans*, *124*, 1717–1735. https://doi.org/10.1029/2018JC014582

Ducet, N., Le Traon, P. Y., & Reverdin, G. (2000). Global high-resolution mapping of ocean circulation from TOPEX/Poseidon and ERS-1 and -2. *Journal of Geophysical Research*, *105*(C8), 19,477–19,498. https://doi.org/10.1029/2000JC900063

Fairall, C. W., Bradley, E. F., Rogers, D. P., Edson, J. B., & Young, G. S. (1996). Bulk parameterization of air-sea fluxes for Tropical Ocean-Global Atmosphere Coupled-Ocean Atmosphere Response Experiment. *Journal of Geophysical Research*, *101*(C2), 3747–3764. https://doi.org/10.1029/95JC03205

Frajka-Williams, E., Rhines, P. B., & Eriksen, C. C. (2009). Physical controls and mesoscale variability in the Labrador Sea spring phytoplankton bloom observed by Seaglider. *Deep-Sea Research Part I: Oceanographic Research Papers*, *56*(12), 2144–2161. https://doi.org/10.1016/j.dsr.2009.07.008

Gordon, H. R., & McCluney, W. R. (1975). Estimation of the depth of sunlight penetration in the sea for remote sensing. *Applied Optics*, *14*(2), 413. https://doi.org/10.1364/ao.14.000413

Halo, I., Penven, P., Backeberg, B., Ansorge, I., Shillington, F., & Roman, R. (2014). Mesoscale eddy variability in the southern extension of the East Madagascar Current: Seasonal cycle, energy conversion terms, and eddy mean properties. *Journal of Geophysical Research: Oceans*, *119*, 7324–7356. https://doi.org/10.1002/2014JC009820

Hood, R. R., Bates, N. R., Capone, D. G., & Olson, D. B. (2001). Modeling the effect of nitrogen fixation on carbon and nitrogen fluxes at BATS. *Deep Sea Research Part II: Topical Studies in Oceanography*, *48*(8-9), 1609–1648. https://doi.org/10.1016/S0967-0645(00)00160-0

Hood, R. R., Coles, V. J., & Capone, D. G. (2004). Modeling the distribution of Trichodesmium and nitrogen fixation in the Atlantic Ocean. *Journal of Geophysical Research*, *109*, C06006. https://doi.org/10.1029/2002JC001753

Hood, R. R., Michaels, A. F., & Capone, D. G. (2000). Answers sought to the enigma of marine nitrogen fixation, Eos. *Transactions American Geophysical Union*, *81*(13), 133. https://doi.org/10.1029/00EO00086

Huhn, F., von Kameke, A., Pérez-Muñuzuri, V., Olascoaga, M. J., & Beron-Vera, F. J. (2012). The impact of advective transport by the South Indian Ocean Countercurrent on the Madagascar plankton bloom. *Geophysical Research Letters*, *39*, L06602. https://doi.org/10.1029/2012GL051246

Lévy, M., Ferrari, R., Franks, P. J., Martin, A. P., & Riviére, P. (2012). Bringing physics to life at the submesoscale. *Geophysical Research Letters*, *39*, L14602. https://doi.org/10.1029/2012GL052756

Lévy, M., Shankar, D., Andrè, J. M., Shenoi, S. S., Durand, F., & de Boyer Montégut, C. (2007). Basin-wide seasonal evolution of the Indian Ocean's phytoplankton blooms. *Journal of Geophysical Research*, *112*, C12014. https://doi.org/10.1029/2007JC004090

Lambert, E., Le Bars, D., & De Ruijter, W. P. M. (2016). The connection of the Indonesian Throughflow, South Indian Ocean Countercurrent and the Leeuwin Current. *Ocean Science*, *12*(3), 771–780. https://doi.org/10.5194/os-12-771-2016

Large, W. G., McWilliams, J. C., & Doney, S. C. (1994). Oceanic vertical mixing: A review and a model with a nonlocal boundary layer parameterization. *Reviews of Geophysics*, *32*, 363–403. https://doi.org/10.1029/94RG01872

Lavender, S., Jackson, T., & Sathyendranath, S. (2015). The Ocean Colour Climate Change Initiative: Merging ocean colour observations seamlessly. *Ocean Challenge*, *21*(1), 29–31.

Lemarié, F., Kurian, J., Shchepetkin, A. F., Jeroen Molemaker, M., Colas, F., & McWilliams, J. C. (2012). Are there inescapable issues prohibiting the use of terrain-following coordinates in climate models? *Ocean Modelling*, *42*, 57–79. https://doi.org/10.1016/j.ocemod.2011.11.007

Lett, C., Verley, P., Mullon, C., Parada, C., Brochier, T., Penven, P., & Blanke, B. (2008). A Lagrangian tool for modelling ichthyoplankton dynamics. *Environmental Modelling and Software*, *23*(9), 1210–1214. https://doi.org/10.1016/j.envsoft.2008.02.005

Lin, I., Liu, W. T., Wu, C. C., Wong, G. T., Hu, C., Chen, Z., et al. (2003). New evidence for enhanced ocean primary production triggered by tropical cyclone. *Geophysical Research Letters*, *30*(13), 1718. https://doi.org/10.1029/2003GL017141

Longhurst, A. (2001). A major seasonal phytoplankton bloom in the Madagascar Basin. *Deep-Sea Research Part I: Oceanographic Research Papers*, *48*(11), 2413–2422. https://doi.org/10.1016/S0967-0637(01)00024-3

Lutjeharms, J. R. (1981). Spatial scales and intensities of circulation in the ocean areas adjacent to South Africa, Deep Sea Research Part A. *Oceanographic Research Papers*, *28*(11), 1289–1302. https://doi.org/10.1016/0198-0149(81)90035-2

Lutjeharms, J. R., & Machu, E. (2000). An upwelling cell inshore of the East Madagascar Current. *Deep-Sea Research Part I: Oceanographic Research Papers*, *47*(12), 2405–2411. https://doi.org/10.1016/S0967-0637(00)00026-1

Machu, E., Lutjeharms, J. R. E., Webb, A. M., & Van Aken, H. M. (2002). First hydrographic evidence of the southeast Madagascar upwelling cell. *Geophysical Research Letters*, *29*(21), 2009. https://doi.org/10.1029/2002GL015381

Marchesiello, P., Debreu, L., & Couvelard, X. (2009). Spurious diapycnal mixing in terrain-following coordinate models: The problem and a solution. *Ocean Modelling*, *26*(3-4), 156–169. https://doi.org/10.1016/j.ocemod.2008.09.004

Menezes, V. V., Phillips, H. E., Schiller, A., Bindoff, N. L., Domingues, C. M., & Vianna, M. L. (2014). South Indian countercurrent and associated fronts. *Journal of Geophysical Research: Oceans*, *119*, 6763–6791. https://doi.org/10.1002/2014JC010076

Naik, R. K., George, J. V., Soares, M. A., Devi, A., Anilkumar, N., Roy, R., et al. (2015). Phytoplankton community structure at the juncture of the Agulhas Return Front and Subtropical Front in the Indian Ocean sector of Southern Ocean: Bottom-up and top-down control. *Deep-Sea Research Part II: Topical Studies in Oceanography*, *118*, 233–239. https://doi.org/10.1016/j.dsr2.2015.01.002

Ou, H.-W., & de Ruijter, W. P. M. (1986). Separation of an inertial boundary current from a curved coastline. *Journal of Physical Oceanography*, *16*(2), 280–289.

Owens, W. B., & Wong, A. P. (2009). An improved calibration method for the drift of the conductivity sensor on autonomous CTD profiling floats by θ–S climatology. *Deep Sea Research Part I*, *56*(3), 450–457. https://doi.org/10.1016/j.dsr.2008.09.008

Palastanga, V., van Leeuwen, P. J., Schouten, M. W., & de Ruijter, W. P. M. (2007). Flow structure and variability in the subtropical Indian Ocean: Instability of the South Indian Ocean Countercurrent. *Journal of Geophysical Research*, *112*, C01001. https://doi.org/10.1029/2005JC003395

Penven, P., Marchesiello, P., Debreu, L., & Lefévre, J. (2008). Software tools for pre- and post-processing of oceanic regional simulations. *Environmental Modelling and Software*, *23*(5), 660–662. https://doi.org/10.1016/j.envsoft.2007.07.004

Ponsoni, L., Aguiar-González, B., Ridderinkhof, H., & Maas, L. R. M. (2016). The East Madagascar Current: Volume Transport and Variability Based on Long-Term Observations*. *Journal of Physical Oceanography*, *46*(4), 1045–1065. https://doi.org/10.1175/JPO-D-15-0154.1

Poulton, A. J., Stinchcombe, M. C., & Quartly, G. D. (2009). High numbers of Trichodesmium and diazotrophic diatoms in the southwest Indian Ocean. *Geophysical Research Letters*, *36*, L15610. https://doi.org/10.1029/2009GL039719

Quartly, G. D., & Srokosz, M. A. (2002). SST Observations of the Agulhas and East Madagascar retroflections by the TRMM microwave imager. *Journal of Physical Oceanography*, *32*(5), 1585–1592. https://doi.org/10.1175/1520-0485(2002)032<1585:SOOTAA>2.0.CO;2

Raj, R. P., Peter, B. N., & Pushpadas, D. (2010). Oceanic and atmospheric influences on the variability of phytoplankton bloom in the Southwestern Indian Ocean. *Journal of Marine Systems*, *82*(4), 217–229. https://doi.org/10.1016/j.jmarsys.2010.05.009

Ramanantsoa, J. D., Krug, M., Penven, P., Rouault, M., & Gula, J. (2018). Coastal upwelling south of Madagascar: Temporal and spatial variability. *Journal of Marine Systems*, *178*(October 2017), 29–37. https://doi.org/10.1016/j.jmarsys.2017.10.005

Ridgway, K. R., Dunn, J. R., & Wilkin, J. L. (2002). Ocean interpolation by four-dimensional weighted least squares—Application to the waters around Australasia. *Journal of Atmospheric and Oceanic Technology*, *19*(9), 1357–1375.

Sapiano, M. R., Brown, C. W., Schollaert Uz, S., & Vargas, M. (2012). Establishing a global climatology of marine phytoplankton phenological characteristics. *Journal of Geophysical Research*, *117*, C08026. https://doi.org/10.1029/2012JC007958

Satyendranath, S., Brewin, R., Brockmann, C., Brotas, V., Ciavatta, S., Chuprin, A., et al. (2016). Creating an ocean-colour time series for use in climate studies: The experience of the ocean-colour climate change initiative. *Remote Sensing of Environment*.

Shchepetkin, A. F., & McWilliams, J. C. (2005). The regional oceanic modeling system (ROMS): A split-explicit, free-surface, topography-following-coordinate oceanic model. *Ocean Modelling*, *9*(4), 347–404. https://doi.org/10.1016/j.ocemod.2004.08.002

Shi, W., & Wang, M. (2007). Observations of a Hurricane Katrina-induced phytoplankton bloom in the Gulf of Mexico. *Geophysical Research Letters*, *34*, L11607. https://doi.org/10.1029/2007GL029724

Siedler, G., Rouault, M., Biastoch, A., Backeberg, B., Reason, C. J. C., & Lutjeharms, J. R. E. (2009). Modes of the southern extension of the East Madagascar Current. *Journal of Geophysical Research*, *114*, C01005. https://doi.org/10.1029/2008JC004921

Siedler, G., Rouault, M., & Lutjeharms, J. R. (2006). Structure and origin of the subtropical South Indian Ocean Countercurrent. *Geophysical Research Letters*, *33*, L24609. https://doi.org/10.1029/2006GL027399

Srokosz, M. A., & Quartly, G. D. (2013). The Madagascar Bloom: A serendipitous study. *Journal of Geophysical Research: Oceans*, *118*, 14–25. https://doi.org/10.1029/2012JC008339

Srokosz, M. A., Quartly, G. D., & Buck, J. J. H. (2004). A possible plankton wave in the Indian Ocean. *Geophysical Research Letters*, *31*, L13301. https://doi.org/10.1029/2004GL019738

Srokosz, M. A., Robinson, J., McGrain, H., Popova, E. E., & Yool, A. (2015). Could the Madagascar bloom be fertilized by Madagascan iron? *Journal of Geophysical Research: Oceans*, *120*, 5790–5803. https://doi.org/10.1002/2015JC011075

Subrahmanyam, B., Rao, K. H., Srinivasa Rao, N., Murty, V. S. N., & Sharp, R. J. (2002). Influence of a tropical cyclone on chlorophyll-a concentration in the Arabian Sea. *Geophysical Research Letters*, *29*(22), 2065. https://doi.org/10.1029/2002GL015892

Uz, B. M. (2007). What causes the sporadic phytoplankton bloom southeast of Madagascar? *Journal of Geophysical Research*, *112*, C09010. https://doi.org/10.1029/2006JC003685

Voldsund, A., Aguiar-González, B., Gammelsrød, T., Krakstad, J.-O., & Ullgren, J. (2017). Observations of the East Madagascar Current system. *Journal of Marine Research*, *75*(4), 531–555. https://doi.org/10.1357/002224017821836725

Wilson, C., & Qiu, X. (2008). Global distribution of summer chlorophyll blooms in the oligotrophic gyres. *Progress in Oceanography*, *78*(2), 107–134. https://doi.org/10.1016/j.pocean.2008.05.002

Wong, A. P. S., Johnson, G. C., & Owens, W. B. (2003). Delayed-mode calibration of autonomous CTD profiling float salinity data by θ S climatology. *Journal of Atmospheric and Oceanic Technology*, *20*(2), 308–318. https://doi.org/10.1175/1520-0426(2003)020<0308:DMCOAC>2.0.CO;2

Yamagami, Y., & Tozuka, T. (2015). Interannual variability of South Equatorial Current bifurcation and western boundary currents along the Madagascar coast. *Journal of Geophysical Research: Oceans*, *120*, 8551–8570. https://doi.org/10.1002/2015JC011069

Zhang, Z., Lowe, R., Ivey, G., Xu, J., & Falter, J. (2016). The combined effect of transient wind-driven upwelling and eddies on vertical nutrient fluxes and phytoplankton dynamics along Ningaloo Reef, Western Australia. *Journal of Geophysical Research: Oceans*, *121*, 4994–5016. https://doi.org/10.1002/2016JC011791